Journal of Nuclear Materials 393 (2009) 141–145

Contents lists available at ScienceDirect

Journal of Nuclear Materials

journal homepage: www.elsevier.com/locate/jnucmat

Density-functional study of Zr-based actinide alloys: 2. U–Pu–Zr system

A. Landa [a,*], P. Söderlind [a], P.E.A. Turchi [a], L. Vitos [b], A. Ruban [b]

[a] Lawrence Livermore National Laboratory, Livermore, CA 94551, USA
[b] Royal Institute of Technology, SE-10044, Stockholm, Sweden

ARTICLE INFO

Article history:
Received 14 February 2009
Accepted 26 May 2009

ABSTRACT

Density-functional theory, previously used to describe phase equilibria in the U–Zr alloys [A. Landa, P. Söderlind, P.E.A. Turchi, L. Vitos, A. Ruban, J. Nucl. Mater. 385 (2009) 68], is applied to study ground-state properties of the bcc U–Pu–Zr solid solutions. Calculated heats of formation of the Pu–U and Pu–Zr alloys are in a good agreement with CALPHAD assessments. We found that account for spin–orbit coupling is important for successful description of Pu-containing alloys.

1. Introduction

In our previous paper, Ref. [1], we performed a detailed *ab initio* study of the main thermodynamic properties of the U–Zr alloy system that is a good nuclear fuel candidate for fast breeder reactors. Although the thermal conductivity of U–Zr alloys is one of the highest among nuclear fuels, the radial temperature gradient generated in fast breeder reactors appears to be sufficiently large to cause redistribution of the alloy constituents [2,3]. The constituent redistribution alters alloy composition during irradiation, which affects local power production, variation in fission product generation, and irradiation behavior such as fuel swelling and growth.

Though the U–Zr alloys can be used as nuclear fuel, a fast rector operation on a closed fuel cycle will, due to the nuclear reactions, contain significant amount of plutonium [3]. It is believed that Pu presence in the U–Pu–Zr alloy at levels greater than 8 wt% enhances U and Zr migration [3–5]. The constituent redistribution in the specific U–19Pu–10Zr (wt%), or $U_{61}Pu_{16}Zr_{23}$ (at.%), alloy was studied in numerous publications [2–6]. This alloy is known to form: (i) a bcc solid solution (γ-phase) in the temperature range of 650–750 °C; (ii) a mixture of γ- and cubic ζ-phases in the temperature range of 600–650 °C; and (iii) below 600 °C the γ-phase transforms to the fcc δ-phase and a mixture of δ- and ζ phase that exists in the temperature range of 500–600 °C [4,5]. A detailed study of the microstructure of the irradiated U–19Pu–10Zr (wt%) alloy [4–6] revealed three distinct concentric zones: the pure γ-phase Zr-enriched porous central zone, the Zr-depleted intermediate zone ($\gamma + \zeta$ mixture), and a slightly Zr-enriched zone on the periphery ($\delta + \zeta$ mixture), while the Pu composition remains almost constant in all three zones with a slight decrease toward the fuel surface. Even though both irradiated U–Zr and U–Pu–Zr alloys develop a porous Zr-enriched central and apparently dense Zr-depleted intermediate zone, a key difference exists in their microstructure [3]. In the irradiated U–Pu–Zr fuel the intermediate zone is almost completely depleted of Zr that migrates both radially inward (to the central zone) and outward (to the periphery). In contrast, evidence of outward Zr migration has not been found yet in the irradiated binary U–Zr fuel: the depleted intermediate zone retains a fair amount of Zr, and the amount of Zr lost from the depleted intermediate zone balances the amount gained in the enriched center [3]. The complex nature of constituent redistribution in the U–Pu–Zr alloys during irradiation and its influence on nuclear fuel performance makes the study of this phenomenon highly relevant.

Recent semi-empirical model calculations [2], supported by experimental observation, indicated that the excess enthalpy of solution of the bcc γ-U–Zr phase controls the constituent redistribution process. In our previous paper [1], we performed detailed calculations of the heat of formation of γ-U–Zr solid solutions. In this work we present results of similar calculations for γ-Pu–U and γ-Pu–Zr alloys that can be used for further analysis of the constituent redistribution in the central zone of U–Pu–Zr nuclear fuels.

In our calculations we employ three complementary computational techniques: (i) a scalar-relativistic (SR) Green function technique based on the Korringa–Kohn–Rostoker (KKR) method within the atomic-sphere approximation (ASA), (ii) scalar-relativistic and fully-relativistic (FR) exact muffin–tin orbital methods (EMTO), and (iii) the all-electron full-potential linear muffin–tin orbital method (FPLMTO) that also accounts for all relativistic effects. Pertinent details of the computational methods are described in Section 2. Results of the density-functional calculations of the ground-state properties of the γ-Pu–U and γ-Pu–Zr solid solutions are presented in Section 3. We provide discussion in Section 4. Lastly, concluding remarks are presented in Section 5.

* Corresponding author. Tel.: +1 925 424 3523; fax: +1 925 422 2851.
E-mail address: landa1@llnl.gov (A. Landa).

0022-3115/$ - see front matter © 2009 Elsevier B.V. All rights reserved.
doi:10.1016/j.jnucmat.2009.05.014

2. Computational details

The calculations we have referred to as SR-KKR-ASA are performed using the SR Green function technique based on the KKR method within the ASA [7–10]. For the present study this approximation is improved by including higher multipoles of the charge density [9] and the so-called muffin–tin correction [10] to the electrostatic energy. The calculations are performed for a basis set including valence *spdf* orbitals. For the electron exchange and correlation energy functional, the generalized gradient approximation (GGA) is considered [11]. Integration over the Brillouin zone is performed using the special *k*-point technique [12] with 506 points in the irreducible wedge of the zone for the bcc structure. The moments of the density of states, needed for the kinetic energy and valence charge density, are calculated by integrating the Green function over a complex energy contour (with a 2.5 Ry diameter) using a Gaussian integration technique with 30 points on a semi-circle enclosing the occupied states. The equilibrium atomic density of the U–Zr, Pu–U, and Pu–Zr alloys is obtained from a Murnaghan [13] fit to the total energy versus lattice constant curve.

In order to treat compositional disorder the SR-KKR-ASA method is combined with the coherent potential approximation (CPA) [14]. The ground-state properties of the chemically random U–Zr, Pu–U, and Pu–Zr alloys are obtained from SR-KKR-ASA-CPA calculations that include the Coulomb screening potential and energy [15–17]. The screening constants are determined from supercell calculations using the locally self-consistent Green function (LSGF) method [18]. The α and β screening constants see Refs. [15,16] for details, are found to be 0.70 and 1.06, 0.93 and 1.17, and 0.57 and 0.81, for U–Zr, Pu–U, and Pu–Zr alloys, respectively.

The SR-KKR-ASA-CPA formalism was very successful for describing the ground-state properties of the U–Zr alloys [1], however the present study reveals that relativistic effects are important for Pu-containing systems. Because of this we use the Green function technique, based on the EMTO formalism, which is not restricted to specific geometries as imposed by the ASA, and also includes the spin–orbit coupling through the four-component Dirac equation [19].

The EMTO calculations are performed using both scalar-relativistic and full relativistic Green's function techniques based on the improved screened KKR method, where the one-electron potential is represented by optimized overlapping muffin–tin (OOMT) potential spheres [20,21]. Inside the potential spheres the potential is spherically symmetric, and it is constant between the spheres. The radii of the potential spheres, the spherical potentials inside the spheres, and the constant value in the interstitial region are determined by minimizing (i) the deviation between the exact and overlapping potentials, and (ii) the errors caused by the overlap between the spheres. Within the EMTO formalism, the one-electron states are calculated exactly for the OOMT potentials. As an output of the EMTO calculations, one can determine self-consistent Green's function of the system and the complete, non-spherically symmetric charged density. Finally, the total energy is calculated using the full charge-density technique [22]. Like in the case of SR-KKR-ASA calculations, GGA is used for the electron exchange and correlation approximation, and EMTO is combined with the CPA for the calculation of the total energy of chemically random alloys [23]. Integrations over the Brillouin zone and complex energy contour and the choice of the screening constants are identical to those in the SR-KKR-ASA method. Although spin-polarization was not considered in the case of the U–Zr system (non-magnetic solution), the Pu–U and Pu–Zr alloys have been modeled within the disordered local moment approximation that leads to a paramagnetic solution, see Ref. [24] for details.

For the elemental metals, the most accurate and fully-relativistic calculations are performed using an all-electron approach where the relativistic effects, including spin–orbit coupling, are accounted for. Although unable to model disorder in the CPA sense it provides important information for the metals, and also serves to confirm the CPA calculations mentioned above. For this purpose we use a version of the FPLMTO [25–27], and the 'full potential' in FPLMTO refers to the use of non-spherical contributions to the electron charge density and potential. This is accomplished by expanding the charge density and potential in cubic harmonics inside non-overlapping muffin–tin spheres and in a Fourier series in the interstitial region. We use two energy tails associated with each basis orbital, and for U's semi-core 6*s*, 6*p* states and valence states (7*s*, 7*p*, 6*d*, and 5*f*) these pairs are different. With this 'double basis' approach we use a total of six energy tail parameters and a total of 12 basis functions per atom. Spherical harmonic expansions are carried out up to $l_{max} = 6$ for the basis, potential, and charge density. As in the case of the SR-KKR-ASA and EMTO methods, GGA is used for the electron exchange-correlation approximation. A special quasi-random structure (SQS) method, utilizing a 16-atom supercell, was used to treat the compositional disorder within the FPLMTO formalism [28]. Spin polarization for the Pu-containing alloys was arranged in an antiferromagnetic fashion [29] with neighboring atoms having anti-parallel spins. This is different from the spin configuration used in the EMTO calculations.

3. Ground-state properties of γ-U–Pu–Zr solid solutions

Fig. 1(a) shows results of SR-KKR-ASA-CPA calculations of the heat of formation of the γ-U–Zr solid solutions at $T = 0$ K [1]. The heat of formation, that shows a positive deviation from the energy associated with a mixture of the pure elements, agrees well with the existence of a miscibility gap in the U–Zr phase diagram. Notice that the calculated heat of formation of the γ-U–Zr solid solutions is in excellent agreement with data derived from a CALPHAD assessment [30–32] of the experimental thermodynamics and phase diagram information, which validates the *ab initio* approach. Note that to have a consistent comparison between the *ab initio* and CALPHAD results, the heat of formation within CALPHAD is also taken at $T = 0$ K, here and in the following discussions on the other two binary systems. For comparison, we also show the heats of formation for the $U_{75}Zr_{25}$, $U_{50}Zr_{50}$, and $U_{25}Zr_{75}$ bcc alloys, calculated within the FPLMTO-SQS technique that agrees pretty well with both SR-KKR-ASA-CPA and CALPHAD assessment results.

Fig. 1(b) shows results of SR-KKR-ASA-CPA, SR-EMTO-CPA, and FR-EMTO-CPA calculations of the heat of formation of the γ-Pu–U solid solutions at $T = 0$ K. Both scalar-relativistic approaches (SR-KKR-ASA-CPA and SR-EMTO-CPA) reveal a positive heat of formation that is in a stark contrast with CALPHAD [32] and FPLMTO-SQS results also shown in this figure. Only when spin–orbit coupling is accounted for within the framework of FR-EMTO-CPA formalism, the calculated heat of formation becomes negative and in excellent agreement with CALPHAD results [32]. In order to understand why the spin–orbit interaction plays an important role in describing the energetics of Pu–U alloys, we present the calculated equilibrium atomic volumes of bcc Pu and U in the Table 1. This table also lists the calculated equilibrium atomic volume of bcc Zr as well as experimental atomic volumes of bcc Pu, U, and Zr [33]. There is a reasonable agreement between the equilibrium atomic volume of bcc U calculated by different approaches. This is not true in the case of bcc Pu, where both SR-KKR-ASA-CPA and SR-EMTO-CPA methods give a significantly larger equilibrium atomic volume than the one calculated within the fully-relativistic approaches (FR-EMTO-CPA and FPLMTO-SQS). The *f*-band occupation in Pu, calculated within the scalar-relativistic formalisms (SR-KKR-

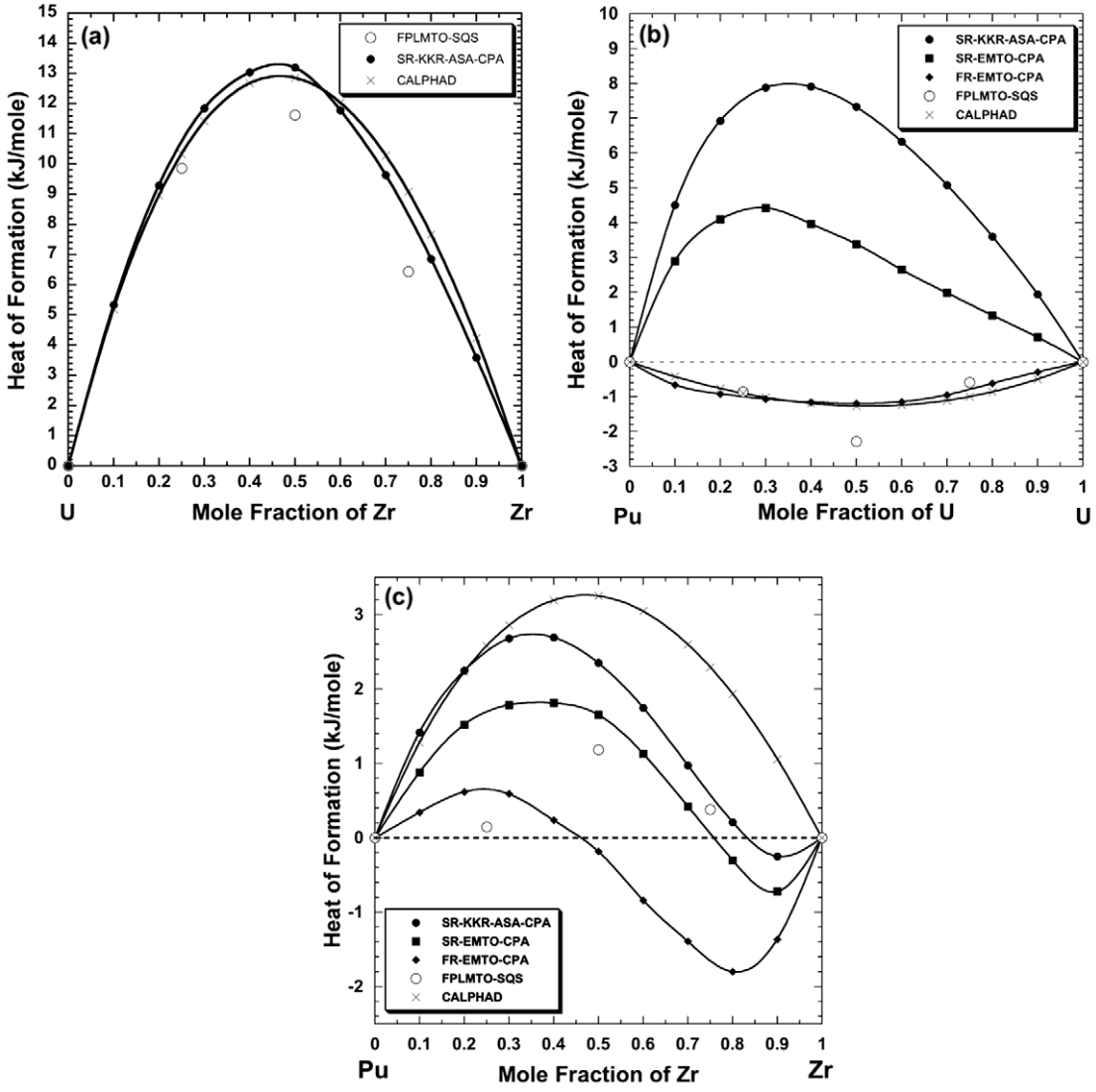

Fig. 1. Heat of formation (in kJ/mole) versus composition for the γ-U–Zr (a), γ-Pu–U (b), and γ-Pu–Zr (c) alloys (T = 0 K).

Table 1
Equilibrium atomic volume (in nm^3) of bcc Pu, U, and Zr. f- and d-band occupations are shown in parentheses for actinides (Pu and U) and Zr, respectively.

Metal	SR-KKR-ASA	SR-EMTO	FR-EMTO	FPLMTO	Experiment [33]
Pu	0.02782 (5.36)	0.02614 (5.40)	0.02405 (5.24)	0.02330 (5.11)	0.02441
U	0.02108 (2.91)	0.02096 (2.98)	0.02125 (2.89)	0.02041 (2.75)	0.02207
Zr	0.02346 (2.65)	0.02293 (2.70)	0.02293 (2.70)	0.02276 (2.40)	0.02350

ASA-CPA and SR-EMTO-CPA), which is also presented in the Table 1 (in the parenthesis), is about 5.4 that is higher than the 5.1–5.2 calculated when spin–orbit coupling is taken into consideration within the FR-EMTO-CPA and FPLMTO-SQS methods. The latter values are in excellent agreement with the photoelectron spectroscopy estimation [34] as well as recent DMFT results [35]. The present study allows us to conclude that spin–orbit coupling becomes crucially important for calculating the excess thermodynamic characteristics of Pu-containing alloys.

Fig. 1(c) shows results of SR-KKR-ASA-CPA, SR-EMTO-CPA, FR-EMTO-CPA, and FPLMTO-SQS calculations of the heat of formation of the γ-Pu–Zr solid solutions at T = 0 K. All CPA-related models reveal a change in the sign of the heat of formation as a function of alloy composition with a tendency towards phase formation for Zr-rich alloys. However this energetic evolution is in contrast with the CALPHAD results [32]. One plausible explanation is that the CALPHAD results were obtained from data for the high-temperature part of the Pu–Zr phase diagram. Therefore it is likely that the γ-phase is primarily stabilized by entropy. It is also worth noting that in all cases the extremum heat of formation is small (note the energy scale compared to the one for U–Zr or Pu–U case), hence reinforcing the assumption that the bcc phase is mainly stabilized by entropy at high temperatures. Comparing results of the EMTO calculations reveals that spin–orbit interaction has also a significant effect in the Pu–Zr system, although not as strong as it is appears for Pu–U alloys. We believe that a fully-relativistic treatment is necessary for an accurate determination of the energetics of all Pu-based alloys.

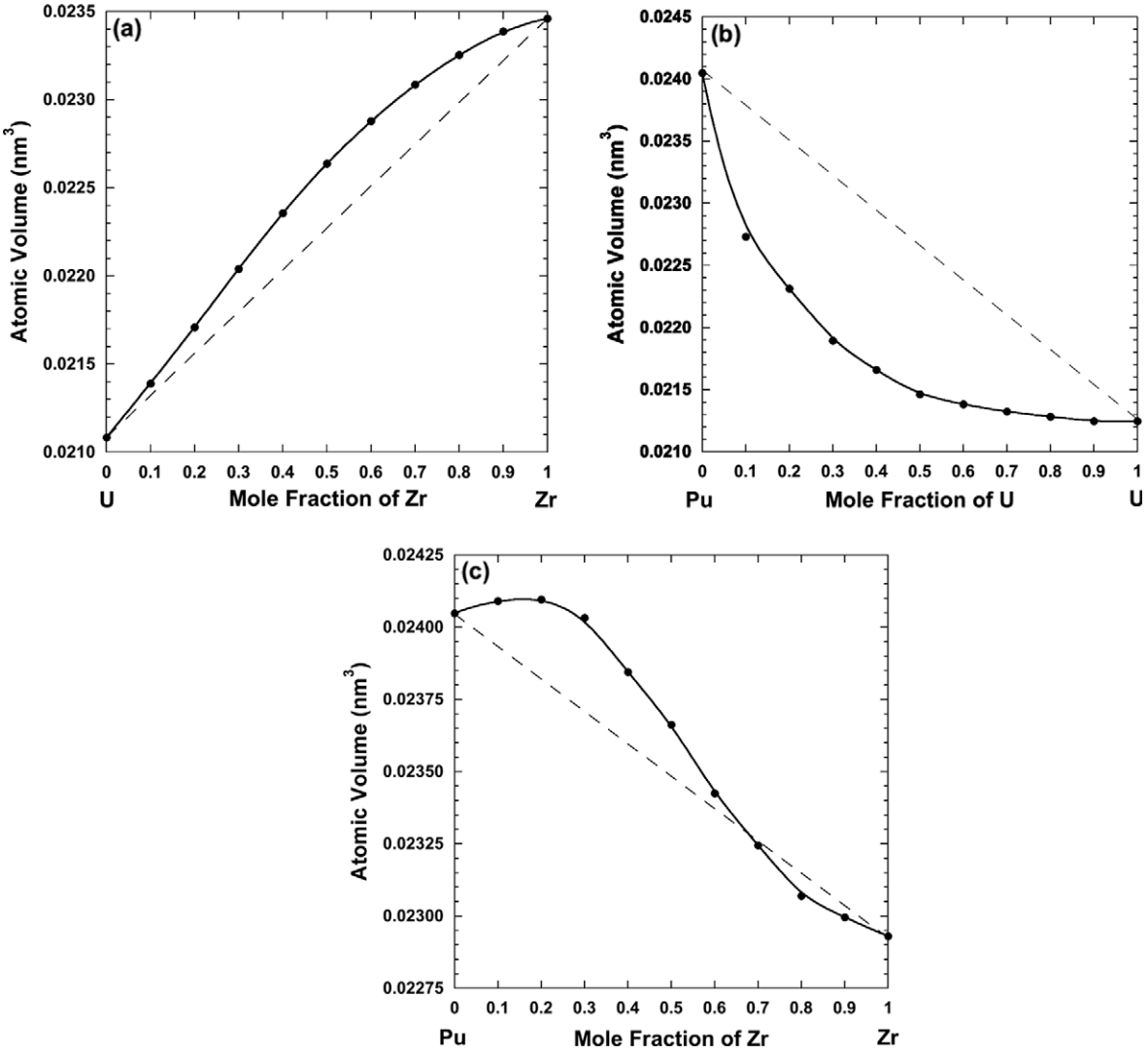

Fig. 2. Atomic volume (in nm^3) versus composition for the γ-U–Zr (a), γ-Pu–U (b), and γ-Pu–Zr (c) alloys (T = 0 K). Calculations for the U–Zr alloys are performed within SR-KKR-ASA-CPA method and for Pu–U and Pu–Zr alloys within FR-EMTO-CPA method.

Fig. 2 shows results of calculations of the equilibrium atomic volume of the bcc U–Zr, Pu–U, and Pu–Zr alloys at T = 0 K. There is a positive deviation from Vegard's law for the γ-U–Zr alloys (results of SR-KKR-ASA-CPA calculations) that is in accord with the positive heat of formation in this system. Results of FR-EMTO-CPA calculations for the γ-Pu–U alloys, shown in this figure, indicate a negative deviation from Vegard's law that agrees well with the negative formation energy of these alloys. The sign change in the deviation from Vegard's law for the γ-Pu–Zr system correlates well with the composition dependence of the formation energy of these alloys.

4. Discussion

As was mentioned in Refs. [3,36], fuel-cladding interdiffusion could be significantly enhanced by lanthanides fission products that are present in increasing amount with higher burnup that could lead to regions with lower melting temperatures in the fuel, effectively thinning the cladding. The main goal of fast spectrum breeder reactors is to achieve high burn-up by fissioning all types of transuranic elements with complete transmutation of long-lived minor actinides, with the result of creating a closed nuclear fuel cycle with future disposition of the nuclear fuel waste products in a single geological repository [37]. Our *ab initio* results will be used to re-assess with the CALPHAD approach the phase diagrams of the binary constituents of the ternary U–Pu–Zr system, and will serve as a template to investigate a mixture of U and Pu with lanthanide fusion products, La, Ce, Pr, Nd, and Sm, and long-lived minor actinides, Np, Am, and Cm, for which experimental data are sparse or lacking. That is why the improved and validated coupling between *ab initio* and CALPHAD methodologies, that we plan to accomplish, will allow us to predict the thermodynamic driving force, associated with any actinide-based alloys, and this will be used as an input for predicting microstructure evolution and site redistribution, and help to validate the development of phenomenological interatomic potentials for subsequent molecular dynamics simulations.

5. Conclusion

In the present paper *ab initio* results are obtained for the U–Pu–Zr alloys to understand the effectiveness of first-principles methods in describing actinide alloys. Ground-state properties of the bcc U–Zr, Pu–U, and Pu–Zr solid solutions were calculated. These *ab initio* results will be used to build a thermodynamic database with important input from first-principles theory will be directly

comparable to the results obtained solely from experimental data on thermodynamic properties and phase diagram.

Both experimental data as well as theoretical results have uncertainties associated with their collection or calculation. The accuracy of the theoretical data is first of all limited to inherent errors of the density-functional-theory approach. For actinide metals, DFT is known to describe the ground-state phases rather well [38]. Phases stable at higher temperatures are more difficult to treat directly from DFT as this is a ground-state theory, but for both U and Pu metals the bcc phase appears to be reasonably well described [29,39]. Pu metal is best approximated within the DFT as a material with finite spin and orbital magnetic moments. It has been argued that the highest temperature phases are stable above the critical temperature of magnetic disorder [24] and the most relevant DFT description reflects this. Here, however, we show that both an antiferromagnetic as well as disordered magnetic configuration for Pu produces similar heat of formation energies. Also relaxation effects associated with the substitutional components can play a role but an analysis of this is beyond present computational capabilities.

Acknowledgements

This work was performed under the auspices of the US Department of Energy by Lawrence Livermore National Laboratory under contract DE-AC52-07NA27344.

References

[1] A. Landa, P. Söderlind, P.E.A. Turchi, L. Vitos, A. Ruban, J. Nucl. Mater. 385 (2009) 68.
[2] G.L. Hofman, S.L. Hayes, M.C. Petri, J. Nucl. Mater. 227 (1996) 277.
[3] G.L. Hofman, L.C. Walters, T.H. Bauer, Prog. Nucl. Energy 31 (1/2) (1997) 83.
[4] Y.H. Sohn, M.A. Dayananda, G.L. Hofman, R.V. Strain, S.L. Hayes, J. Nucl. Mater. 279 (2000) 317.
[5] Yeon Soo Kim, G.L. Hofman, S.L. Hayes, Y. H Sohn, J. Nucl. Mater. 327 (2004) 27.
[6] Yeon Soo Kim, S.L. Hayes, G.L. Hofman, A.M. Yacout, J. Nucl. Mater. 359 (2006) 17.
[7] O. Gunnarson, O. Jepsen, O.K. Andersen, Phys. Rev. B 27 (1983) 7144.
[8] I.A. Abrikosov, H.L. Skriver, Phys. Rev. B 47 (1993) 16532.
[9] A.V. Ruban, H.L. Skriver, Comput. Mater. Sci. 15 (1999) 119.
[10] N.E. Christensen, S. Satpathy, Phys. Rev. Lett. 55 (1985) 600.
[11] J.P. Perdew, K. Burke, M. Ernzerhof, Phys. Rev. Lett. 77 (1996) 3865.
[12] D.J. Chadi, M.L. Cohen, Phys. Rev. B 8 (1973) 5747; Phys. Rev. B 39 (1989) 3168.
[13] F.D. Murnaghan, Natl. Acad. Sci. USA 30 (1944) 244.
[14] J.S. Faulkner, Prog. Mater. Sci. 27 (1982) 1.
[15] A.V. Ruban, H.L. Skriver, Phys. Rev. B 66 (2002) 024201.
[16] A.V. Ruban, S.I. Simak, P.A. Korzhavyi, H.L. Skriver, Phys. Rev. B 66 (2002) 024202.
[17] A.V. Ruban, S.I. Simak, S. Shallcross, H.L. Skriver, Phys. Rev. B 67 (2003) 214302.
[18] I.A. Abrikosov, S.I. Simak, B. Johansson, A.V. Ruban, H.L. Skriver, Phys. Rev. B 56 (1997) 9319.
[19] L.V. Pourovskii, A.V. Ruban, L. Vitos, H. Ebert, B. Johansson, I.A. Abrikosov, Phys. Rev. B 71 (2005) 094415.
[20] L. Vitos, Phys. Rev. B 64 (2001) 014107.
[21] L. Vitos, Computational Quantum Mechanics for Materials Engineers: The EMTO Method and Application, Springer, London, 2007.
[22] J. Kollar, L. Vitos, H.L. Skriver, in: H. Dreyssé (Ed.), Electronic Structure and Physical Properties of Solids: The Uses of the LMTO Method, Lecture Notes in Physics, Springer, Berlin, 2000, p. 85.
[23] L. Vitos, I.A. Abrikosov, B. Johansson, Phys. Rev. Lett. 87 (2001) 156401.
[24] P. Söderlind, A. Landa, B. Sadigh, Phys. Rev. B 66 (2002) 205109; A. Landa, P. Söderlind, J. Alloys Compd. 354 (2003) 99.
[25] J.M. Wills, B. Cooper, Phys. Rev. B 36 (1987) 3809.
[26] D.L. Price, B. Cooper, Phys. Rev. B 39 (1989) 4945.
[27] J.M. Wills, O. Eriksson, M. Alouani, D.L. Price, in: H. Dreyssé (Ed.), Electronic Structure and Physical Properties of Solids: The Uses of the LMTO Method, Lecture Notes in Physics, Springer, Berlin, 2000, p. 148.
[28] A. Zunger, S.H. Wei, L.G. Ferreira, J.E. Bernard, Phys. Rev. Lett. 65 (1990) 353.
[29] P. Söderlind, Europhys. Lett. 55 (2001) 525; P. Söderlind, B. Sadigh, Phys. Rev. Lett. 92 (2004) 185702.
[30] P.E.A. Turchi, I.A. Abrikosov, B. Burton, S.G. Fries, G. Grimvall, L. Kauffman, P. Korzhavyi, V. Rao Manga, M. Ohno, A. Pisch, A. Scott, W. Zhang, CALPHAD 31 (2007) 4.
[31] M. Kurata, T. Ogata, K. Nakamura, T. Ogawa, J. Alloys Compd. 271/273 (1998) 636.
[32] M. Kurata, CALPHAD 23 (1999) 315.
[33] J. Donohue, The Structures of the Elements, John Wiley, New York, 1974.
[34] J.G. Tobin, P. Söderlind, A. Landa, K.T. Moore, A.J. Schwartz, B.W. Chung, M.A. Wall, J.M. Wills, R.G. Haire, A.L. Kutepov, J. Phys. Condens. Matter 20 (2008) 125204.
[35] J.H. Shim, K. Haule, G. Kotliar, Nature 446 (2007) 513.
[36] J.D. Petti, D. Crawford, N. Chauvin, MRS Bulletin 34 (1) (2009) 40.
[37] D. D Keiser Jr, J.B. Kennedy, B.A. Hilton, S.L. Hayes, JOM 1 (2008) 29.
[38] P. Söderlind, Adv. Phys. 47 (1998) 959.
[39] C.-S. Yoo, H. Cynn, P. Söderlind, Phys. Rev. B 57 (1998) 10359.